Original Article
ISSN (Online): 2582-7472

ShodhKosh: Journal of Visual and Performing Arts
April 2024 5(4), 1506–1517

PHOTOCATALYTIC REMOVAL OF TOXIC TEXTILE DYES FROM WATER USING CU-DOPED ZNO NANOPARTICLES UNDER NATURAL SUNLIGHT

D. Sonia [1], E.K. Kirupa Vasam [2]

[1] Research Scholar (Reg no: 20123112032018), Department of Chemistry & Research Centre, Nesamony Memorial Christian College, Marthandam-629165(Affiliated to Manonmaniam Sundaranar University, Abishekapatti, Tirunelveli), Tamilnadu, India
[2] Assistant Professor, Department of Chemistry & Research Centre, Nesamony Memorial Christian College, Marthandam-629165(Affiliated to Manonmaniam Sundaranar University, Abishekapatti, Tirunelveli), Tamilnadu, India

DOI
10.29121/shodhkosh.v5.i4.2024.4441

Funding: This research received no specific grant from any funding agency in the public, commercial, or not-for-profit sectors.

ABSTRACT

An efficient copper-doped ZnO (Cu-doped ZnO) nanoparticle was synthesized in nano form via co-precipitation using zinc sulfate heptahydrate as a precursor. The synthesized Cu-doped ZnO nanoparticle was characterized using X-ray diffraction (XRD), FT-IR, UV-DRS, SEM with EDX, and HRTEM techniques. The bandgap energy of the Cu-doped ZnO nanoparticle was reduced, enhancing visible-light absorption. The addition of copper ions modified the electronic and optical properties of the photocatalyst, thereby improving its photocatalytic performance. The photocatalytic activity of Cu-doped ZnO nanoparticles was evaluated for the degradation of Direct Red 81 dye (DR-81) as a pollutant in an aqueous solution. Under optimal conditions (DR-81 dye concentration of 20 ppm, Cu-doped ZnO dosage of 0.4 g/100 mL, and 60 minutes of sunlight irradiation), a maximum DR-81 removal efficiency of approximately 70.83% was achieved. A plausible photocatalytic degradation mechanism of DR-81 using Cu-doped ZnO was proposed, revealing that $\bullet O_2^-$ and •OH radicals were the primary active species responsible for its degradation. Cyclic experiments demonstrated the high stability and reusability of Cu-doped ZnO, confirming its potential as an economical and environmentally friendly photocatalyst.

Graphical Abstract

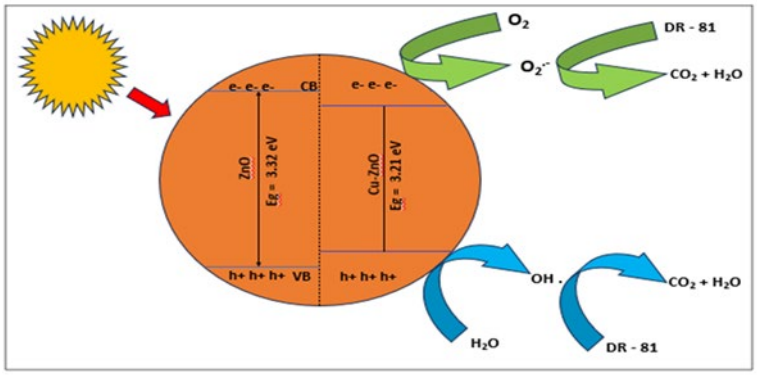

Keywords: Cu-doped ZnO, Photocatalyst, Nanoparticle, Direct Red 81, Photocatalytic Removal, Sunlight

1. INTRODUCTION

Population growth, rapid industrial expansion, and lifestyle changes have all contributed to the growing scarcity of resources. As a result of increasing waste generated by industries and individuals, effective waste management has become essential [1]. Researchers have focused on ecological processes that promote waste reduction, reuse, and

recycling to achieve a closed-loop material cycle by utilizing waste-derived resources. Dye pollution from the textile and paper industries is a major environmental concern [2]. Conventional treatment of dye-contaminated wastewater often involves flocculation or coagulation. Among dye types used for textile fibers, reactive dyes have the lowest exhaustion levels due to their low substantivity to the substrate and high sensitivity to hydrolysis under alkaline dyeing conditions [3, 4]. Dyes are organic compounds frequently found in wastewater from the textile industry. When released into natural water bodies, they can overload the water's self-purification mechanisms, inhibit or halt photosynthetic processes, and pose harmful effects, including carcinogenic risks, to aquatic ecosystems [5-7]. Direct Red 81 dye is widely used across numerous industries [8, 9] and can cause harm to the skin and eyes. However, the release of raw DR-81 dye into waterways may pose a significant threat to public health [10]. In water, DR-81 poses several health risks to humans. Due to their high solubility, dyes can easily disperse through rivers, altering water quality. Therefore, industrial effluents must be treated to remove such hazardous dyes before they contaminate freshwater sources.

Recent research suggests that advanced oxidation processes (AOPs), particularly photocatalytic techniques, are highly effective for treating industrial wastewater. The efficiency of these approaches is attributed to the generation of active species, such as hydroxyl radicals (•OH), which degrade contaminants into harmless by-products like water and carbon dioxide [11-13]. Photocatalytic reactions occur when ultraviolet (UV) or visible light strikes the surface of a semiconductor catalyst (e.g., TiO_2 and ZnO). These processes excite electrons in the valence band, transferring them to the conduction band. The resulting electron-hole (e/h) pairs in the catalyst oxidize pollutant molecules by generating additional hydroxyl radicals and facilitating oxidation and regeneration reactions [14-16]. Recent studies have focused on zinc oxide (ZnO) nanoparticles (NPs) as semiconductor catalysts due to their high chemical stability, low toxicity, excellent optical and electrical properties, and strong oxidizing potential. These nanoparticles have been widely used for the decomposition and oxidation of persistent organic pollutants [17-19]. However, a major limitation of ZnO NPs is their high rate of electron-hole recombination, which reduces photocatalytic efficiency [20].

In general, overcoming photocatalyst limitations is essential for improving their performance and expanding practical applications. One promising approach that has gained increasing research interest is the doping of ZnO NPs with transition metals such as cobalt (co), silver (Ag), iron (Fe), gold (Au), and copper (Cu) [21]. Doping ZnO with an appropriate dopant can tune its bandgap energy and suppress charge carrier recombination (electron-hole pairs), thereby enhancing its effectiveness in the photocatalytic and sonocatalytic degradation of organic and hazardous contaminants [22-24].

In this context, Isai et al. [25] reported that Fe-doped ZnO exhibited enhanced optical absorption and significant photocatalytic activity for the degradation of methylene blue dye. In a separate study, Chang et al. [26] examined the light absorption capacity, electron-hole pair separation, and photocatalytic efficiency of cerium-doped ZnO nanoparticles (NPs) and observed improvements. Building on this background, the present study aims to investigate the efficacy of Cu-doped ZnO NPs in removing Direct Red 81 dye under visible light irradiation. Various nanomaterial synthesis methods have been reported, including sol-gel, co-precipitation, hydrothermal, thermal hydrolysis, and DC thermal plasma synthesis [27]. However, among these, the co-precipitation method is preferred for its superior photocatalytic activity [28]. Additionally, this synthesis approach offers a low-cost, eco-friendly solution for industrial wastewater purification.

This study synthesized undoped ZnO and Cu-doped ZnO photocatalysts using the co-precipitation method. The synthesized photocatalyst had a wurtzite phase structure and a band gap of 3.21 eV, which is lower than that of undoped ZnO. Within 60 minutes of irradiation, the Cu-doped ZnO photocatalyst mineralized Direct Red 81 (DR 81), an organic dye contaminant. It also exhibited high stability and reusability. Thus, our study established a novel method for synthesizing a modified metal-doped ZnO photocatalyst for the remediation of emerging industrial contaminants.

2. EXPERIMENTAL SECTIONS

2.1. CHEMICALS AND MATERIALS

All chemical reagents used in this study were analytical grade. Zinc sulfate heptahydrate ($ZnSO_4 \bullet 7H_2O$), copper sulfate pentahydrate ($CuSO_4 \bullet 5H_2O$), and potassium hydroxide (KOH) were purchased from LOBA Chemie. Double-distilled water was used for all experiments. Direct Red 81 dye (DR-81, $C_{29}H_{19}N_5Na_2O_8S_2$) was used as the pollutant for the present study and was purchased from Sigma-Aldrich.

2.2. SYNTHESIS OF UNDOPED ZNO AND CU-DOPED ZNO NANOPARTICLES

All chemical reagents used in this study were analytical grade. $ZnSO_4 \bullet 7H_2O$, $CuSO_4 \bullet 5H_2O$, and potassium hydroxide were acquired from LOBA Chemie. The coprecipitation approach was used to prepare both undoped and Cu-doped zinc oxide nanoparticles. A stoichiometric amount of zinc sulfate heptahydrate ($ZnSO_4 \bullet 7H_2O$) was dissolved in 100 mL of distilled water. To increase the pH, a 1 M KOH solution was added dropwise to the solution and stirred continuously for around 6 hours. The resulting suspension was centrifuged, washed with double-distilled water and ethanol, dried at 120°C for 12 hours, and then calcined in a muffle furnace at 500°C for 2 hours. To synthesize Cu-doped ZnO photocatalysts, a stoichiometric amount of zinc sulfate heptahydrate ($ZnSO_4 \bullet 7H_2O$) was dissolved in 100 mL of distilled water. Copper sulfate pentahydrate ($CuSO_4 \bullet 5H_2O$) was added to the solution and stirred continuously. The pH of the solution was then adjusted by adding 1 M KOH solution dropwise. Stirring continued for about 6 hours, and the precipitate was filtered, washed, dried, and calcined under the same conditions used to synthesize undoped ZnO to obtain the Cu-doped ZnO nanoparticles [29].

2.3. CHARACTERIZATION

The crystallography of the undoped ZnO and Cu-doped ZnO nanoparticles was studied using an X-ray diffractometer (XRD) with CuKα irradiation (λ = 0.154 nm), operated at 40 kV and 100 mA, in the diffraction range (2θ) of 20°–80°. The vibrational spectrum was monitored using an FT-IR spectrometer (8400S, Shimadzu, Japan) in the wavenumber range of 4000–400 cm^{-1}. The surface morphology and shape of undoped ZnO and Cu-doped ZnO nanoparticles were examined using a scanning electron microscope (JEOL, 5800LV) with energy-dispersive X-ray spectroscopy (JSM-7100F) to determine the chemical composition of the nanoparticles. The morphology and average size of the nanoparticles were determined using HRTEM (JEOL-2100). A double-beam spectrophotometer was used to analyze the optical absorption properties using UV-Vis diffuse reflectance spectroscopy (Agilent Cary 5000) in the 200–800 nm wavelength range.

2.4. PHOTOCATALYTIC ACTIVITY

The photocatalytic activity of synthesized undoped ZnO and Cu-doped ZnO nanoparticles was evaluated by measuring the photocatalytic degradation of an aqueous solution of Direct Red-81 dye in the presence of sunlight at neutral pH. Initially, 20 ppm of dye solution was added to a reactor, followed by a small dose of undoped ZnO and Cu-doped ZnO NPs (0.4 g/100mL). The suspension was stirred in the dark for 30 minutes to achieve absorption-desorption equilibrium, then placed in direct sunlight with constant stirring. An aliquot of the test solution was extracted at regular intervals, centrifuged, and the concentration of the sample was determined using a UV-visible spectrophotometer. The following equation was used to calculate dye degradation efficiency [25].

$$\% \text{ Degradation} = (C_0 - C_t)/C_0 \times 100 \quad \text{----------} \quad (1)$$

C_0 refers to the initial concentration of the test solution with adsorption-desorption equilibrium and C_t denotes the concentration of the solution after photocatalytic degradation.

3. RESULTS AND DISCUSSION

3.1. X-RAY DIFFRACTION ANALYSIS

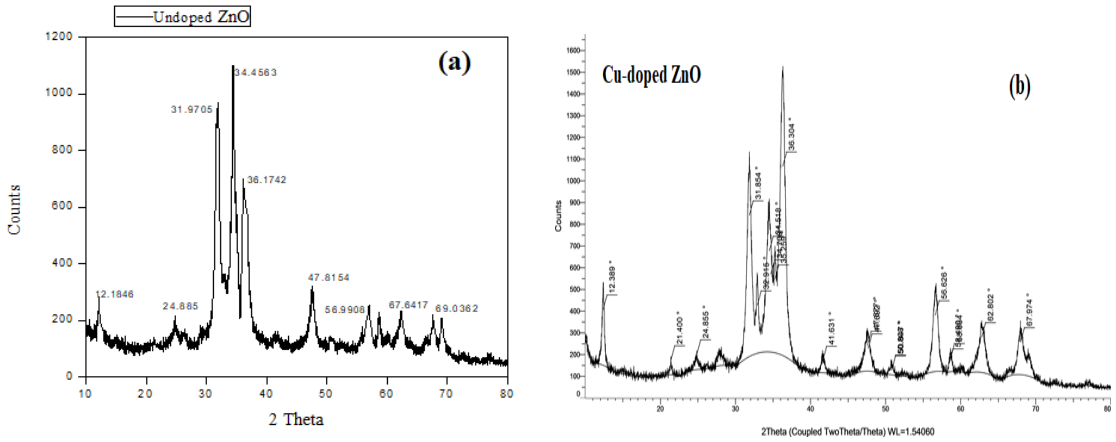

Fig. 1: X-ray diffraction patterns of (a) undoped ZnO and (b) Cu-doped ZnO nanoparticles.

Figure 1(a) and 1(b) show the XRD patterns of undoped and Cu-doped ZnO nanoparticles. Three broad peaks were observed at 2θ = 31.9705°, 34.4565°, and 36.1742° for undoped ZnO, and at 2θ = 31.854°, 34.709°, and 36.307° for Cu-doped ZnO. The three diffraction peaks correspond to the crystallographic planes (100), (002), and (101) of hexagonal ZnO. The well-defined sharp peaks indicate the high crystalline nature of the undoped ZnO and Cu-doped ZnO nanoparticles. All peaks in the XRD patterns of undoped ZnO and Cu-doped ZnO samples could be matched with the hexagonal wurtzite structure from JCPDS card No. 36-1451 [30, 31]. The broadening of the XRD lines is due to the nanocrystalline nature of the material, indicating that the particle size is in the nanometer range. The average crystalline size of synthesized nanoparticles was calculated using the Scherrer formula, as shown in Eq. (4) [32].

$$D = K\lambda/\beta \cos\theta \quad \text{.....(2)}$$

where D is the average crystalline size, K is the shape factor, lambda is the wavelength in angstroms (Å), β is the FWHM in radians, and theta (θ) is the diffraction angle in degrees. Based on the Scherrer equation, the average crystal size of the undoped ZnO and Cu-doped ZnO nanoparticles was calculated to be 32.01 nm and 23.32 nm, respectively.

3.2. FT-IR ANALYSIS

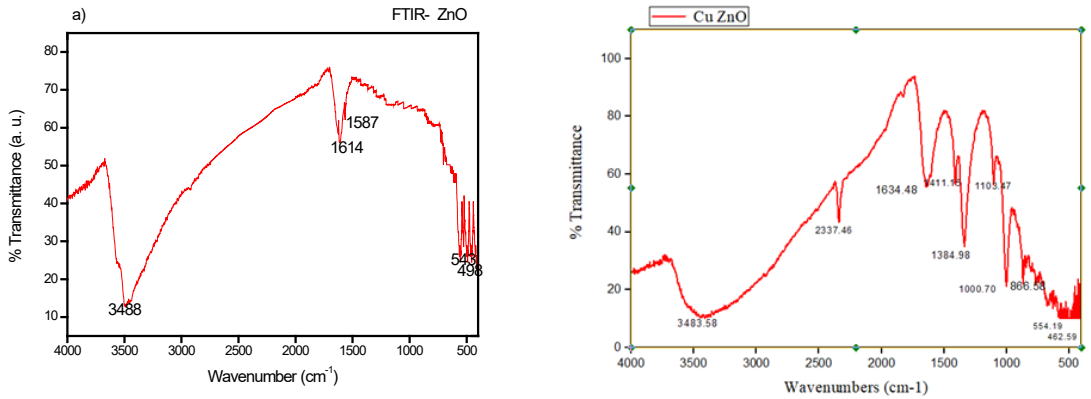

Fig. 2: FT-IR spectra of (a) undoped ZnO and (b) Cu-doped ZnO nanoparticles

The chemical bonds and functional groups of undoped ZnO and Cu-doped ZnO nanoparticles were studied using FT-IR spectroscopy, and the corresponding spectra are illustrated in Fig. 2(a) and 2(b). The vibrational bands at 3480 and 1600 cm^{-1} correspond to the stretching and bending vibrations of O-H observed in the molecule or hydroxyl groups adsorbed on the surfaces of the samples, respectively [33]. The presence of Zn-O stretching vibrations at lower wavenumbers (550-460 cm^{-1}) suggests the formation of the ZnO matrix [34]. In contrast to undoped ZnO, Cu doping has been associated with observable shifts and the emergence of new peaks in the Cu-doped ZnO spectrum. These changes result from the interactions of Cu ions with the ZnO lattice, which can modify the overall bond strength and create localized defects.

3.3. UV-VIS DRS STUDIES

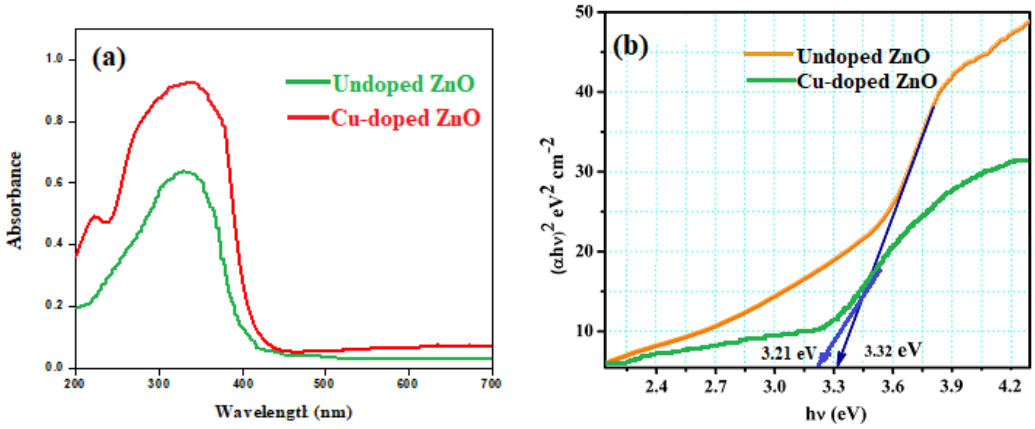

Fig. 3: (a) UV-Vis absorption spectra and (b) Tauc plot of undoped ZnO and Cu-doped ZnO nanoparticles.

The optical absorption spectra of synthesized undoped ZnO and Cu-doped ZnO nanoparticles were examined using UV-Vis DRS at room temperature in the range of 200 to 700 nm, as shown in Figure 3(a). The optical band gap of the nanoparticles was calculated using Tauc's equation, Eq. (1) [35]:

$$\alpha h\nu = A\,(h\nu - Eg)^{n} \quad \text{.....} \quad (3)$$

where, α is the absorption coefficient, $h\nu$ is the photon energy, Eg is the band gap, A is a constant and n refers to the index that depends on the type of electronic transition. The band gap can be determined by extrapolating the straight-line portion of the plot to zero absorbance, i.e. $(\alpha h\nu))^2 = 0$, as shown in Figure 3(b).

The absorption spectrum of undoped ZnO shows maximum absorption at 373 nm. With the addition of Cu, the absorption edge shifts to a higher wavelength (379 nm) compared to undoped ZnO. This shift in the absorption edge may be attributed to the incorporation of Cu into the ZnO matrix, leading to a narrowing of the optical band gap upon Cu doping, as shown in Figure 3(b) [36, 37]. The optical band gap decreases from 3.32 eV for undoped ZnO to 3.21 eV for Cu-doped ZnO.

The decrease in band gap cannot be attributed to structural changes caused by the addition of Cu to ZnO. As our XRD analysis shows, replacing Zn with Cu, which are neighbours in the periodic table, does not result in any substantial change in the crystal structure. The observed red shift in the band gap is due to Cu doping in ZnO. The narrowing of the band gap is explained by *p-d* spin-exchange interactions between the band electrons and the localized *d* electrons of the transition-metal ion that replaces Zn^{2+} with Cu^{2+}. Cu doping reduces the band gap due to the high *p-d* mixing of O and Cu [38]. The red shift in the band gap demonstrates the homogeneous substitution of Cu ions in the ZnO lattice. Furthermore, the narrowing of the band gap is influenced by many-body effects on the conduction and valence bands [39], which may be caused by electron interactions and impurity scattering. This phenomenon has been attributed to the merging of an impurity band with the conduction band, resulting in a smaller band gap.

3.4. SEM ANALYSIS

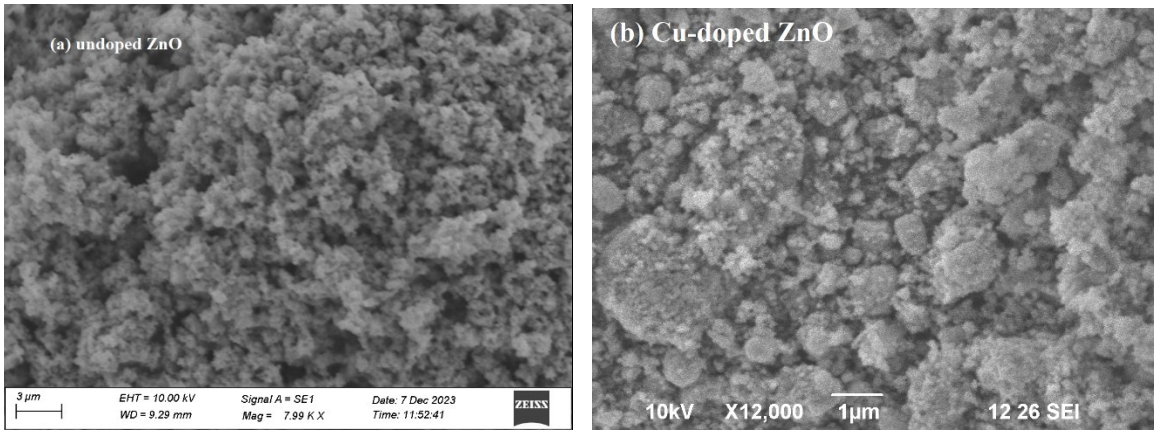

Fig. 4: SEM images of (a) undoped ZnO and (b) Cu-doped ZnO nanoparticles

SEM was used to observe the crystal morphology and surface characteristics of the synthesized samples. The SEM images of undoped ZnO and Cu-doped ZnO nanoparticles are shown in Fig. 4(a) and 4(b). These images indicate that the shape and morphology of ZnO nanoparticles change with Cu ion doping. In the Cu-doped ZnO nanoparticles, the particles appear more agglomerated. This is primarily due to Van der Waals forces, as well as doping-induced changes in polarity and surface charge, which are the main factors contributing to nanoparticle agglomeration [40].

3.5. ENERGY DISPERSIVE X-RAY (EDX) SPECTROSCOPY ANALYSIS

An Energy Dispersive X-ray (EDX) study was conducted to analyze the elemental composition of the synthesized nanoparticles and to confirm successful doping and ZnO nanoparticle formation. The EDX signals and percentage compositions of undoped ZnO and Cu-doped ZnO nanoparticles are shown in Fig. 5(a) and 5(b). For undoped ZnO nanoparticles, sharp signals for zinc and oxygen were observed, confirming the formation of ZnO nanoparticles. For Cu-doped samples, in addition to zinc and oxygen, copper signals were also detected. This confirms the successful incorporation of copper into the ZnO lattice.

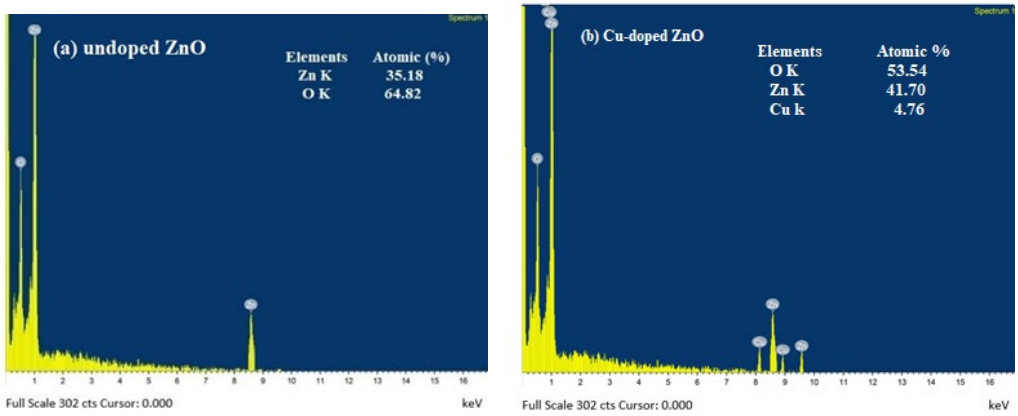

Fig. 5: EDX pattern of (a) undoped ZnO and (b) Cu-doped ZnO nanoparticles.

3.6. TEM ANALYSIS

The shape and particle size of undoped ZnO and Cu-doped ZnO nanoparticles were further analyzed using HR-TEM, which provides direct information about the distribution of metal oxides on the surface. Figures 6(a) and 6(b) present high-resolution TEM images of undoped ZnO and Cu-doped ZnO nanoparticles, respectively. TEM confirms the monodisperse and uniform particle size of the nanoparticles. With Cu doping in ZnO nanoparticles, we observe a clear

contrast enhancement in Figure 6(b) compared to Figure 6(a). This clearly confirms the presence of Cu in the ZnO matrix, which is fully supported by the EDX study. Figure 6(b) illustrates spherical Cu-doped ZnO photocatalyst particles with sizes ranging from 10 to 40 nm. Figures 6(c) and 6(d) present the particle size distribution histograms generated using the Gaussian fitting method, confirming average particle sizes of 32 nm and 23 nm for undoped ZnO and Cu-doped ZnO nanoparticles, respectively. These results are consistent with the XRD data.

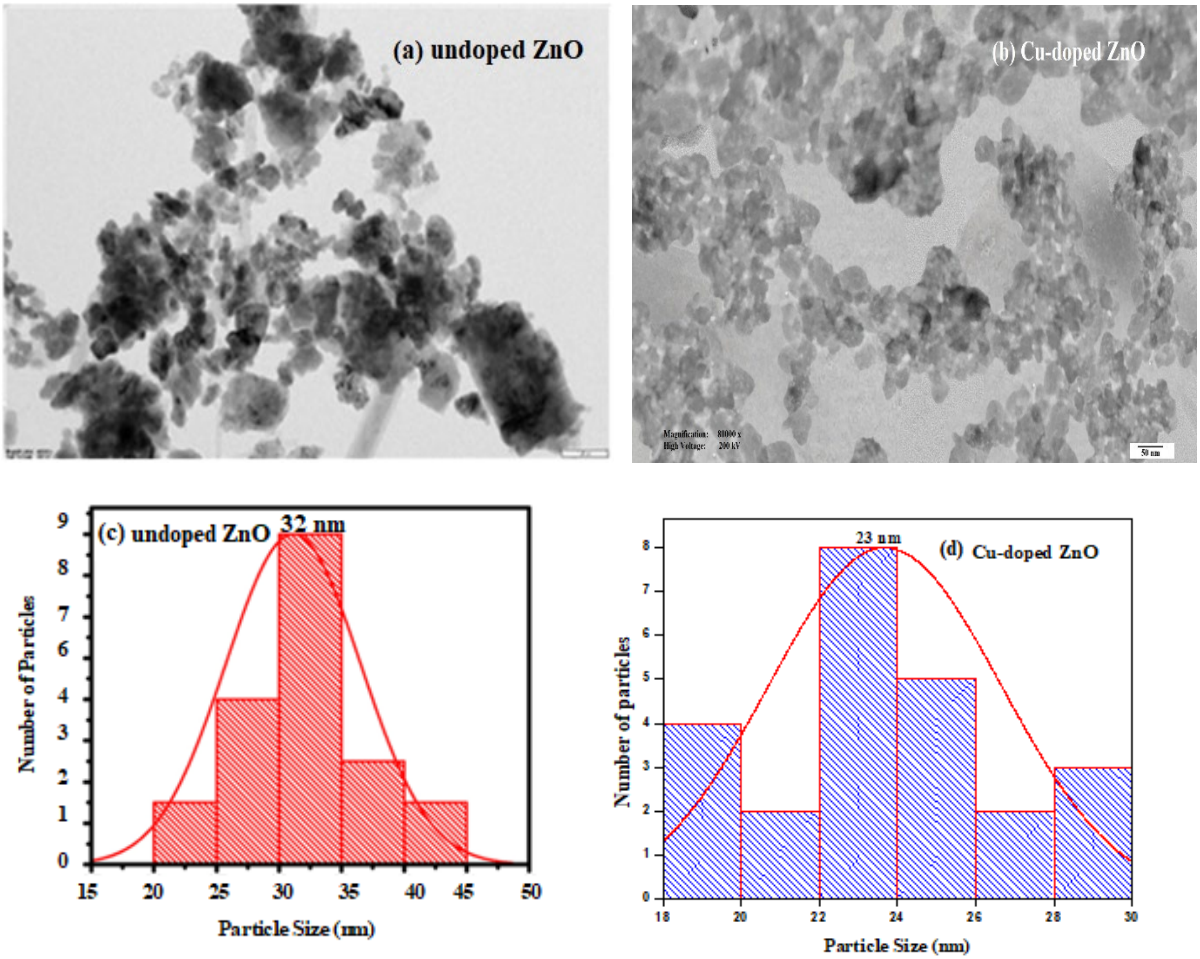

Fig. 6: HR-TEM images of (a) undoped ZnO and (b) Cu-doped ZnO;
Particle size distribution of (c) undoped ZnO and (d) Cu-doped ZnO.

3.7. PHOTOCATALYTIC REMOVAL OF DR-81 DYE

The UV–visible absorption spectra of DR-81 dye with undoped ZnO and Cu-doped ZnO photocatalysts at a dosage of 0.4 g/100 mL and a dye concentration of 20 ppm under solar light irradiation are illustrated in Figures 7a and 7b.The intensity of the main peak of DR-81 declines over various time intervals. The peak intensity decreases due to the photocatalytic degradation of DR-81 in the presence of undoped ZnO and Cu-doped ZnO photocatalysts after 60 minutes of sunlight irradiation. To monitor self-degradation, DR-81 was photolyzed for 60 minutes under sunlight without a photocatalyst (Figure 7c). Compared to the photocatalytic experiment, the DR-81 dye solution exhibits minimal self-degradation [41]. Another set of experiments was conducted in the absence of sunlight to investigate the removal efficiency of DR-81 in the dark due to dye adsorption on the photocatalyst surface. In the dark, the removal efficiencies of DR-81 with undoped ZnO and Cu-doped ZnO photocatalysts are 16% and 32%, respectively.

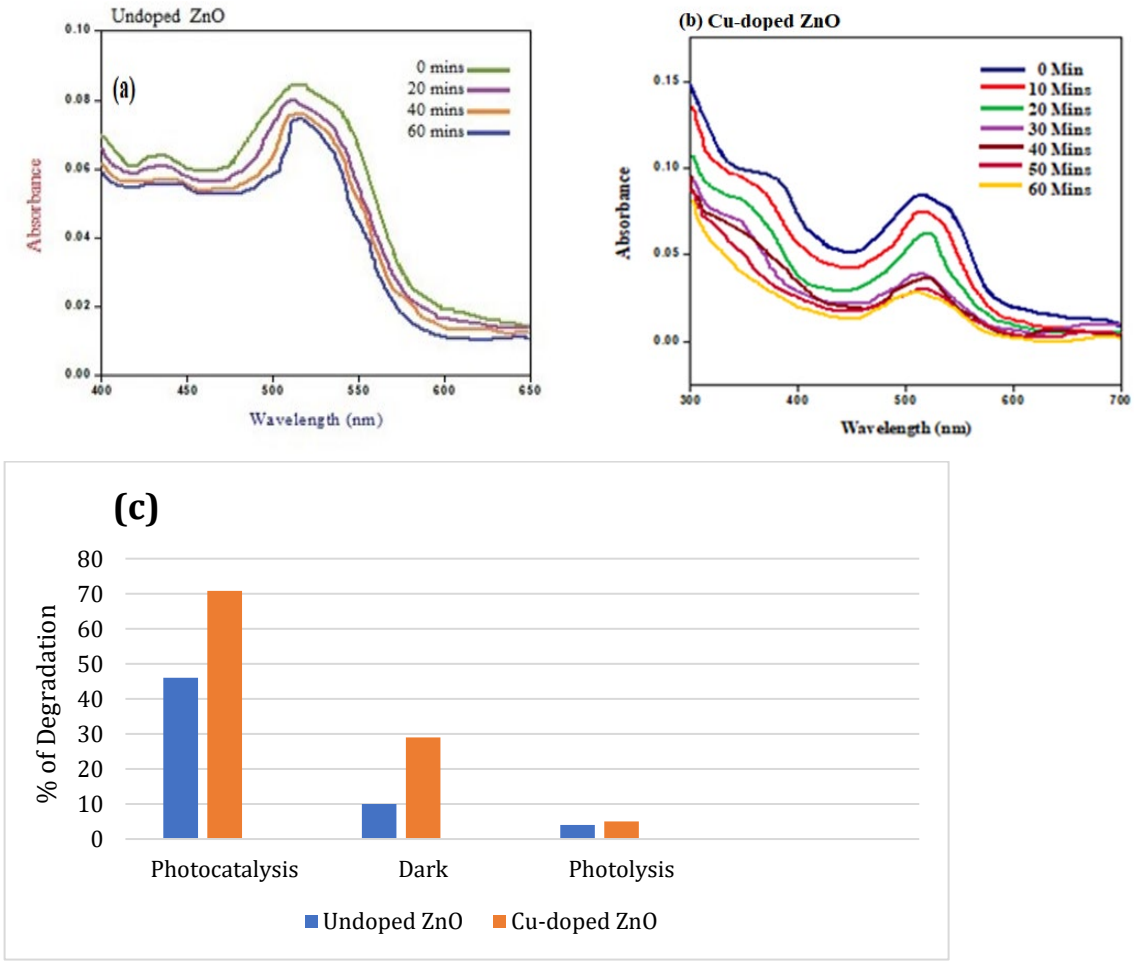

Fig. 7: (a) and (b) UV–visible results showing the decrease in intensity of the DR-81 dye solution, and (c) photocatalytic degradation, adsorption in the dark, and photolysis of DR-81.

Understanding the photocatalytic removal efficiency of synthesized photocatalysts is of great importance. The experiments were conducted using undoped ZnO and Cu-doped ZnO photocatalysts while keeping other parameters constant, as shown in Figure 7c. From the photocatalytic experiments, the DR-81 dye removal efficiencies of undoped ZnO and Cu-doped ZnO photocatalysts were found to be 46% and 70.83%, respectively, after 60 minutes of solar light irradiation. There is a significant increase in the DR-81 dye removal efficiency of Cu-doped ZnO compared to undoped ZnO. This can be attributed to the doping of copper with ZnO, which suppresses the e^-/h^+ recombination rate [41, 42]. Moreover, copper doping can substantially inhibit crystal size growth [43, 44], as confirmed by XRD, thereby increasing photocatalytic activity. Furthermore, the bandgap energy decreases for Cu-doped ZnO, as confirmed by UV-Vis DRS data. Thus, copper incorporation with ZnO results in a synergistic effect, leading to enhanced photocatalytic degradation of DR-81 dye [45, 46].

3.8. PHOTOCATALYTIC DEGRADATION MECHANISM

The photocatalytic degradation of DR-81 dye with Cu-doped ZnO nanoparticles, as shown in Figure 8, proceeds efficiently through a mechanism involving reactive oxygen species (ROS) generation. Upon irradiation with solar light, Cu-doped ZnO absorbs photons, exciting electrons from the valence band (VB) to the conduction band (CB) and generating electron-hole pairs [47], as expressed by Equation 4. Photogenerated holes (h^+) react with water molecules, producing highly reactive hydroxyl radicals (·OH), while electrons (e^-) present in the conduction band reduce dissolved oxygen, resulting in superoxide radicals ($\cdot O_2^-$) [48], as described in Equations 5 and 6. Additionally, superoxide radicals react with protons and electrons to yield hydrogen peroxide (H_2O_2), which further decomposes to form more hydroxyl

radicals, as shown in Equation 7. These ROS, primarily ·OH and $\cdot O_2^-$, facilitate the breakdown of DR-81 dye into degradable products such as carbon dioxide (CO_2) and water (H_2O) [49], as illustrated in Equation 8. Cu doping enhances charge separation and minimizes recombination, ultimately improving photocatalytic activity due to increased ROS generation. The obtained results demonstrate the high efficiency and potential of Cu-doped ZnO nanoparticles for the photocatalytic degradation of organic pollutants in wastewater treatment.

$$Cu\text{-}ZnO + h\nu \rightarrow e^- (CB) + h^+ (VB) \quad \ldots\ldots(4)$$

$$h^+ (VB) + H_2O \rightarrow \cdot OH + H^+ \quad \ldots\ldots(5)$$

$$e^- (CB) + \cdot O_2^- + 2\,H^+ \rightarrow H_2O_2 \quad \ldots\ldots(6)$$

$$e^- (CB) + H_2O_2 \rightarrow \cdot OH + OH^- \quad \ldots\ldots(7)$$

$$\cdot OH / \cdot O_2^- + \text{DR-81} \rightarrow \text{Degraded products } (CO_2 + H_2O + \ldots) \quad \ldots(8)$$

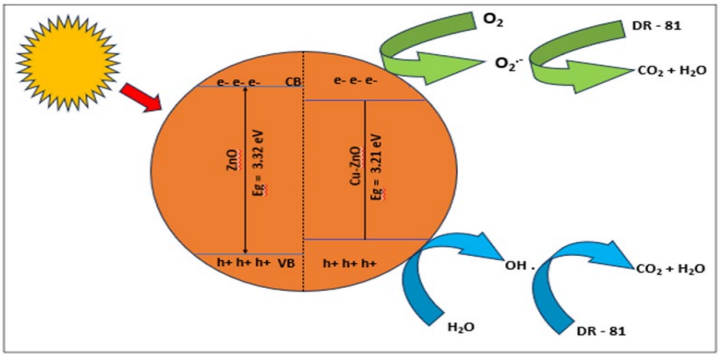

Fig. 8: Schematic diagram of Cu-doped ZnO photocatalytic degradation mechanism

3.9. PHOTOCATALYST REUSABILITY

The reusability of the Cu-doped ZnO photocatalyst was evaluated over five cycles under optimal conditions (initial DR-81 concentration: 20 ppm; photocatalyst amount: 0.4 g/100 mL; irradiation time: 60 min), with the results presented in Figure 9. After each cycle, the used photocatalyst was collected and dried for reuse in the subsequent cycle [50]. The DR-81 removal efficiency of the Cu-doped ZnO photocatalyst exhibited a moderate decline in successive cycles. Due to the poisoning effect of degradation products and the obstruction of solar irradiation, dye removal efficiency significantly decreased over the five cycles [51]. Consequently, it can be concluded that Cu-doped ZnO is suitable for the long-term and repeated removal of dye from textile effluents.

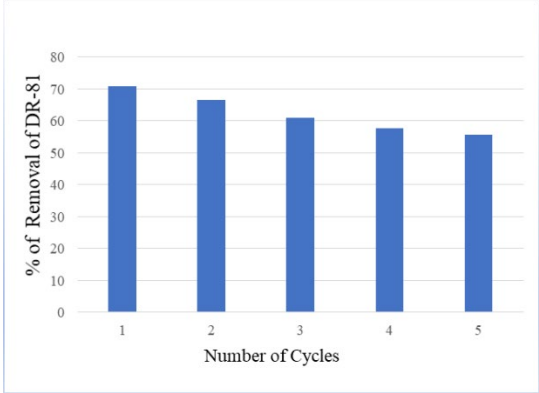

Fig. 9: Photostability and Reusability of Cu-doped ZnO

4. CONCLUSION

Undoped zinc oxide nanoparticles, along with copper-doped zinc oxide nanoparticles, were successfully synthesized using the co-precipitation method for the photocatalytic decomposition of Direct Red 81 under visible light irradiation. The synthesized undoped ZnO and Cu-doped ZnO nanoparticles exhibit crystallite sizes of 32 nm and 23 nm, respectively,

with bandgap energies of 3.32 eV and 3.21 eV. The significant reduction in bandgap energy enhances optical absorption in the visible-light region. The photocatalytic removal efficiency of DR-81 dye using undoped ZnO and Cu-doped ZnO was observed to be 46% and 70.83%, respectively, within 60 minutes of natural sunlight irradiation. These experimental findings reveal that the photocatalytic activity of ZnO nanoparticles in DR-81 dye removal increases after doping with Cu metal compared to the undoped state under visible light irradiation. In other words, these results indicate the efficacy of copper doping in reducing hole-electron recombination, increasing hydroxyl radical (•OH) formation in ZnO, and creating impurity states in the structure of doped ZnO nanoparticles, all of which contribute to the enhanced photocatalytic activity of the synthesized Cu-doped ZnO nanoparticles. Thus, the synthesis of copper-doped ZnO nanophotocatalysts under visible light irradiation presents an efficient and promising technology for the photocatalytic removal of Direct Red 81 dye from aqueous environments.

CONFLICT OF INTERESTS

None.

ACKNOWLEDGMENTS

The authors are thankful for Karunya institute of technology and science, Coimbatore, India, Ayya Nadar Janaki Ammal College, Sivakasi, India; and Alagappa University, Karaikudi, India for furnishing necessary provision and support for this work.

REFERENCES

Chebor LJ (2018) Characterization of synthesized ZnO nanoparticles and their application in photodegradation of methyl orange dye under fluorescent lamp irradiation. Int J Sci Eng Sci2:5–8.

Hossain A, Sadique RABM, Raihan MJ, Nargis A, Ismail IMI, Habib A, Mahmood AJ (2016) Kinetics of degradation of eosin y by one of the advanced oxidation processes (AOPs)-Fenton's process. Am J Anal Chem 7:863–879.

Golob, Vera, Aleksandra Vinder, and Marjana Simonič (2005) Efficiency of the coagulation/flocculation method for the treatment of dyebath effluents. Dyes and pigments 67, 2: 93-97.

Mahmoodi, Niyaz Mohammad, Raziyeh Salehi, Mokhtar Arami, and Hajir Bahrami (2011) Dye removal from colored textile wastewater using chitosan in binary systems. Desalination 267: 64-72.

Zandsalimi Y, Taimori P, Soltani RDC, Rezaee R, Abdullahi N, Safari M (2015) Photocatalytic removal of acid red 88 dye using zinc oxide nanoparticles fixed on glass plates. J Adv Environ Health Res. 3:102–10.

Shirmardi M, Mahvi AH, Mesdaghinia A, Nasseri S, Nabizadeh R. (2013) Adsorption of acid red-18 dye from aqueous solution using single wall carbon nanotubes: kinetic and equilibrium. Desalin Water Treat. 51: 6507–16.

Nadafi K, Vosoughi M, Asadi A, Borna MO, Shirmardi M. (2014) Reactive Red 120 dye removal from aqueous solution by adsorption on nano-alumina. JWater Chem Technol. 36(3):125–33.

Sivakumar B, S. Karthikeyan , C. Kannan. (2010) Film and pore diffusion modeling fortheadsorption of Direct Red 81 on activated carbon prepared from Balsamodendron Caudatum wood waste. Dig J Nanomater Bios. 5:657-665.

Heravi MM, Zari Abasion, Ali Morsali1, Pouran Ardalan and Touran Ardalan. (2015) Biosorption of Direct Red 81 dye from aqueous solution on prepared Sonchus fruit plant, as a low cost biosorbent: thermodynamic and kinetic study. J Appl Chem, 9:17-22.

Chollom MN, Rathila S, Pillay V L, Dorcas Alfa. (2015) The applicability of nanofiltration for the treatment and reuse of textile reactive dye effluent. Water SA, 41: 398-405.

Ajmal A, Majeed I, Malik R, Iqbal M, Nadeem MA, Hussain I. (2016) Photocatalytic degradation of textile dyes on Cu2O-CuO/TiO2 anatase powders. J Environ Chem Eng. 4:2138–46.

Ghaneian MT, Morovati P, Ehrampoush MH, Tabatabaee M. (2014) Humic acid degradation by the synthesized flower-like Ag/ZnO nanostructure as an efficient photocatalyst. J Environ Health Sci Eng.12:138-146.

Zhou K, Hu X-Y, Chen B-Y, Hsueh C-C, Zhang Q, Wang J. (2016) Synthesized TiO2/ZSM-5 composites used for the photocatalytic degradation of azo dye: intermediates, reaction pathway, mechanism and bio-toxicity. Appl Surf Sci. 383:300–9.

Mittal M, Sharma M, Pandey O P. (2014) UV–visible light induced photocatalytic studies of Cu doped ZnO nanoparticles prepared by coprecipitation method. Sol Energy. 110:386–97.

Karimi L, Zohoori S, Yazdanshenas M E. (2014) Photocatalytic degradation of azo dyes in aqueous solutions under UV irradiation using nano-strontium titanate as the nanophotocatalyst. J Saudi Chem Soc. 18:581–8.

Hadi M, McKay G, Samarghandi MR, Maleki A, Solaimany Aminabad M. (2012) Prediction of optimum adsorption isotherm: comparison of chi-square and log-likelihood statistics. DesalinWater Treat. 49:81–94.

Sun L, Yao Y, Wang L, Mao Y, Huang Z, Yao D, Lu W, Chen W. (2014) Efficient removal of dyes using activated carbon fibers coupled with 8-hydroxyquinoline ferric as a reusable Fenton-like catalyst. Chem Eng J 240:413–419

Haydar MS (2015) Photodegradation of Alizarin Black S dye using zinc oxide. J Environ Sci Eng 4:395–400

Samadi M, Zirak M, Naseri A, Khorashadizade E, Moshfegh AZ. (2016) Recent progress on doped ZnO nanostructures for visible-light photocatalysis. Thin Solid Films. 605:2–19.

Xu C, Cao L, Su G, LiuW, Qu X, Yu Y. (2010) Preparation, characterization and photocatalytic activity of Co-doped ZnO powders. J Alloys Compd. 497:373–6.

Subash B, Krishnakumar B, SwaminathanM, Shanthi M. (2013) Synthesis and characterization of cerium–silver co-doped zinc oxide as a novel sunlight-driven photocatalyst for effective degradation of reactive Red 120 dye. Mater Sci Semicond Process. 16:1070–8.

Soltani RDC, Jorfi S, Ramezani H, Purfadakari S. (2016) Ultrasonically induced ZnO–biosilica nanocomposite for degradation of a textile dye in aqueous phase. Ultrason Sonochem. 28:69–78.

Mekasuwandumrong O, Pawinrat P, Praserthdam P, Panpranot J. (2010) Effects of synthesis conditions and annealing post-treatment on the photocatalytic activities of ZnO nanoparticles in the degradation of methylene blue dye. Chem Eng J. 164:77–84.

Maleki A, Shahmoradi B. (2012) Solar degradation of Direct Blue 71 using surface modified iron doped ZnO hybrid nanomaterials. Water Sci Technol. 65:1923–8.

Kalpesh Anil Isai, Vinod Shankar Shrivastava. (2019) Photocatalytic degradation of methylene blue using ZnO and 2%Fe–ZnO semiconductor nanomaterials synthesized by sol–gel method: a comparative study, SN Applied Sciences 1:1247-11.

Chang CJ, Lin CY, Hsu MH. (2014) Enhanced photocatalytic activity of Ce-doped ZnO nanorods under UVand visible light. J Taiwan Inst Chem Eng. 45:1954–63

Sankara Reddy B, Venkatramana Reddy S, Koteeswara Reddy N, Pramoda K J. (2013) Synthesis, Structural, Optical Properties and Antibacterial activity of codoped (Ag, Co) ZnO Nanoparticles. Res. J. Material Sci. 1:11-20.

Fabbiyola S, John Kennedy L,Udaya Aruldoss, Bououdina M, Dakhel A A & Judith Vijaya. (2015) Synthesis of Co-doped ZnO nanoparticles via co-precipitation: Structural, optical and magnetic properties, J Powder Technology. 286:757-765.

Thutiyaporn Thiwawong, Korakot Onlaor, Natpasit Chaithanatkun, and Benchapol Tunhoo, (2018) Preparation of Copper Doped Zinc Oxide Nanoparticles by Precipitation Process for Humidity Sensing Device, International Conference on Science and Technology of Emerging Materials, 020022-1– 020022-5.

Singh N, Mehra RM, Kapoor A (2011) Synthesis and characterization of ZnO nanoparticles. J Nano Electron Phys 3:132–139

Pourrahimi AM, Liu D, Pallon LKH, Andersson RL, Martinez AA, Lagaron JM, Hedenqvist MS, Ström V, Gedde UW, Olsson RT (2014) Water-based synthesis and cleaning methods for high purity ZnO nanoparticles—comparing acetate, chloride, sulphate and nitrate zinc salt precursors. RSC Adv 4:35568–35577

Shokri A, Rabiee F, Mahanpoor K (2017) Employing a novel nanocatalyst (Mn/Iranian hematite) for oxidation of SO2 pollutant in aqueous environment. Int J Environ Sci Technol 14:2485–2494.

K. Bhuvaneswari, G. Palanisamy, K. Sivashanmugan, T. Pazhanivel, T. Maiyalagan, (2021) ZnO nanoparticles decorated multiwall carbon nanotube assisted ZnMgAl layered triple hydroxide hybrid photocatalyst for visible light-driven organic pollutants removal, J. Environ. Chem. Eng. 9:104909-12.

L.P.P. Ha, T.H.T. Vinh, N.T.B. Thuy, C.M. Thi, Viet P. Van, (2021) Visible-light-driven photocatalysis of anisotropic silver nanoparticles decorated on ZnO nanorods: synthesis and characterizations, J. Environ. Chem. Eng. 9:105103-13.

Ghomri R, Nasiruzzaman S, Ahmed, Song W, Cai W, Bououdina, Ghers M. (2018) Pure and (Er, Al) co-doped ZnO nanoparticles: synthesis, characterization, magnetic and photocatalytic properties. Materials in Electronics. 29:10677-7

Y. Jin, Q. Cui, K. Wang, J. Hao, Q. Wang, J. Zhang. (2011) Investigation of photoluminescence in undoped and Ag-doped ZnO flowerlike nanocrystal. J. Appl. Phys. 109:053521-10.

Rajender Singh, P. B. Barman, Dheeraj Sharma, Synthesis. (2017) structural and optical properties of Ag doped ZnO nanoparticles with enhanced photocatalytic properties by photo degradation of organic dyes, J Mater Sci: Mater Electron 28:5705–5717

Ferhat M, Zaoui A, Ahuja R. (2009) Magnetism and band gap narrowing in Cu-doped ZnO. Appl Phys Lett 94:142502-8.

Muhammad Sajjada, Inam Ullaha, M.I. Khanb, Jamshid Khanc, M. Yaqoob Khana, Muhammad Tauseef Qureshi. (2018) Structural and optical properties of pure and copper doped zinc oxide nanoparticles, Results in Physics, 9:1301-1309,

Sharma, P., (2021). Defect engineering in ZnO nanoparticles through metal doping. ACS Applied Materials & Interfaces, 13:1–19

Pant, B.; Ojha, G.P.; Kuk, Y.S.; Kwon, O.H.; Wan Park, Y.; Park, M. (2020) Synthesis and characterization of ZnO-TiO2/carbon fiber composite with enhanced photocatalytic properties. Nanomaterials. 10:1960-11.

Delsouz Khaki, M.R.; Shafeeyan, M.S.; Raman, A.A.A.; Daud, W.M.A.W. (2018) Evaluating the efficiency of nano-sized Cu doped TiO2/ZnO photocatalyst under visible light irradiation. J. Mol. Liq, 258:354–365.

Mulpuri, R.K.; Tirukkovalluri, S.R.; Imandi, M.R.; Alim, S.A.; Lakshmi Kapuganti, V.D. (2019) Zinc and boron co-doped nanotitania with enhanced photocatalytic degradation of acid red 6A under visible light irradiation. Sustain. Environ. Res, 1:29-36.

Li, W.; Wu, D.; Yu, Y.; Zhang, P.; Yuan, J.; Cao, Y.; Cao, Y.; Xu, J. (2014) Investigation on a novel ZnO/TiO2-B photocatalyst with enhanced visible photocatalytic activity. Phys. E Low-Dimens. Syst. Nanostruct. 58:118–123.

Panwar, S.; Upadhyay, G.K.; Purohit, L.P. (2022) Gd-doped ZnO:TiO2 heterogenous nanocomposites for advance oxidation process. Mater. Res. Bull. 145:111534-46.

Mousa, H.M.; Alenezi, J.F.; Mohamed, I.M.A.; Yasin, A.S.; Hashem, A.F.M.; Abdal-hay, A. (2021) Synthesis of TiO2@ZnO heterojunction for dye photodegradation and wastewater treatment. J. Alloys Compd. 886:161169-11.

Tian, J.; Shao, Q.; Zhao, J.; Pan, D.; Dong, M.; Jia, C.; Ding, T.; Wu, T.; Guo, Z. (2019) Microwave solvothermal carboxymethyl chitosan templated synthesis of TiO2/ZrO2 composites toward enhanced photocatalytic degradation of Rhodamine B. J. Colloid Interface Sci. 541:18–29.

Hou, X.; Stanley, S.L.; Zhao, M.; Zhang, J.; Zhou, H.; Cai, Y.; Huang, F.; Wei, Q. (2019) MOF-based C-doped coupled TiO2/ZnO nanofibrous membrane with crossed network connection for enhanced photocatalytic activity. J. Alloys Compd. 777:982–990.

Ahmed, A.Z.; Islam, M.M.; Islam, M.M.u.; Masum, S.M.; Islam, R.; Molla, M.A.I. (2020) Fabrication and characterization of B/Sn-doped ZnO nanoparticles via mechanochemical method for photocatalytic degradation of rhodamine B. Inorg. Nano-Metal Chem. 51:1369–1378.

Molla, M.A.I.; Furukawa, M.; Tateishi, I.; Katsumata, H.; Kaneco, S. (2019) Fabrication of Ag-doped ZnO by mechanochemical combustion method and their application into photocatalytic Famotidine degradation. J. Environ. Sci. Heal. Part A Toxic Hazard. Subst. Environ. Eng. 54: 914–923.

Mondol, B.; Sarker, A.; Shareque, A.M.; Dey, S.C.; Islam, M.T.; Das, A.K.; Shamsuddin, S.M.; Molla, M.A.I.; Sarker, M. (2021) Preparation of Activated Carbon/TiO2 Nanohybrids for Photodegradation of Reactive Red-35 Dye Using Sunlight. Photochem. 1:54–66